Received 31 October 2017
Revised 2 July 2018
Accepted 9 October 2018

Model calibration of locally nonlinear dynamical systems

Extended constitutive relation error with multi-harmonic coefficients

Xiaoyu Hu
Department of Civil Engineering, Clemson University, Clemson, South Carolina, USA

Evan Chodora
Department of Mechanical Engineering, Clemson University, Clemson, South Carolina, USA

Saurabh Prabhu
Client Risk Solutions, AIG, Clemson, South Carolina, USA

Akshay Gupte
Department of Mathematical Sciences, Clemson University, Clemson, South Carolina, USA, and

Sez Atamturktur
Department of Mechanical Engineering, Clemson University, Clemson, South Carolina, USA

Abstract

Purpose – This paper aims to present an approach for calibrating the numerical models of dynamical systems that have spatially localized nonlinear components. The approach implements the extended constitutive relation error (ECRE) method using multi-harmonic coefficients and is conceived to separate the errors in the representation of the global, linear and local, nonlinear components of the dynamical system through a two-step process.

Design/methodology/approach – The first step focuses on the system's predominantly linear dynamic response under a low magnitude periodic excitation. In this step, the discrepancy between measured and predicted multi-harmonic coefficients is calculated in terms of residual energy. This residual energy is in turn used to spatially locate errors in the model, through which one can identify the erroneous model inputs which govern the linear behavior that need to be calibrated. The second step involves measuring the system's nonlinear dynamic response under a high magnitude periodic excitation. In this step, the response measurements under both low and high magnitude excitation are used to iteratively calibrate the identified linear and nonlinear input parameters.

Findings – When model error is present in both linear and nonlinear components, the proposed iterative combined multi-harmonic balance method (MHB)-ECRE calibration approach has shown superiority to the conventional MHB-ECRE method, while providing more reliable calibration results of the nonlinear parameter with less dependency on *a priori* knowledge of the associated linear system.

Originality/value – This two-step process is advantageous as it reduces the confounding effects of the uncertain model parameters associated with the linear and locally nonlinear components of the system.

Keywords Finite element method, Model uncertainty, Constrained minimization, ECL benchmark, Nonlinear model calibration

Paper type Research paper

Engineering Computations
Vol. 36 No. 2, 2019
pp. 466-490

0264-4401
DOI 10.1108/EC-10-2017-0419

1. Introduction

Local nonlinearities are pervasive in engineering applications (Shi and Atluri, 1992; Fey *et al.*, 1996; Wojtkiewicz and Johnson, 2011). In some cases, local nonlinearities are deliberately designed into the system to avoid excessively high responses or stresses (Fey, 1992), and in others, they arise from large deformations or material stress (Clough and Wilson, 1979). Examples include nonlinear bearings (Nelson and Nataraj, 1989), dry friction damping (Ferri and Dowell, 1988), local nonlinear springs and dampers (Qu, 2002), structural joints with an opening and closing ability (Niwa and Clough, 1982) and concrete cracking (Atamturktur *et al.*, 2013; Llau *et al.*, 2015).

In these systems, as the nonlinear effects are localized within a component of a larger linear system, the dynamic response tends to remain predominantly linear for small magnitude forces (Clough and Wilson, 1979). However, when sufficiently high magnitude forces are applied, the dynamic behavior becomes nonlinear and is governed by the interaction between the linear and nonlinear components. Hence, when developing numerical models to represent such systems, one must pay attention to accurate modeling of both the global system that exhibits the underlying linear behavior and the spatially local component that introduces nonlinearity. It is important to note that modeling error in the underlying linear behavior could degrade the prediction accuracy of the overall nonlinear behavior, resulting in large deviations from the measured dynamic response (Lenaerts *et al.*, 2001; Kerschen *et al.*, 2003; Kerschen *et al.*, 2005; Hot, 2012). As such, the accuracy with which model error in local, nonlinear components can be identified is naturally dependent on errors which may be associated with linear components.

Common approaches for calibrating models of nonlinear dynamical systems can be grouped into two categories. The first category of approaches corrects errors in the representation of both the linear and nonlinear responses of the system simultaneously (Lenaerts *et al.*, 2001; Meyer and Link, 2003; Bellizzi and Defilippi, 2003; Kerschen *et al.*, 2005). These approaches may face the identifiability problem due to the large number of confounding parameters that need to be calibrated using an inevitably finite set of available measurements (Lenaerts *et al.*, 2001; Kurt *et al.*, 2005; Jaishi and Ren, 2007; Van Buren and Atamturktur, 2012). The second category of approaches, on the other hand, corrects the representation of only the nonlinear response, and therefore assumes the linear system to be modeled accurately. This assumption in turn mandates the availability of reliable *a priori* knowledge of the linear system (Kerschen *et al.*, 2005; Isasa *et al.*, 2011). Hence, this second approach risks that during calibration of the locally nonlinear component parameters errors in the linear system may be compensated for as the linear model accuracy is seldom guaranteed. Separately identifying the modeling errors that govern the system's linear and nonlinear behavior offers a solution that can mitigate the issues related to identifiability faced by both of these categories of approaches (Lenaerts *et al.*, 2001; Ewins *et al.*, 2015).

In this paper, a two-step process is presented for calibrating numerical models of dynamical systems with local nonlinearities. The process involves separately measuring the system's predominantly linear and nonlinear dynamic response under periodic excitation at low and high force magnitudes, respectively. This is a development over other published approaches that face from the previously mentioned identifiability issues. From these response measurements, multi-harmonic coefficients, a commonly used set of features for characterization of nonlinear dynamical systems (Cardona *et al.*, 1994), are extracted. When coupled with the extended constitutive relation error (ECRE), the multi-harmonic coefficients allow the calculation of the residual energy, which reflects the discrepancy between the model predictions and the experimental measurements (Isasa *et al.*, 2011; Hu *et al.*, 2017). In the first step of this study, the residual energy in the predominantly linear

behavior is calculated for each discretized finite element allowing us to identify the model input parameters that need calibration. These input parameters, when combined with the poorly known parameters associated with the local nonlinearity constitute the total set of calibration parameters.

Subsequently, in the second step, the residual energy calculated under both the low magnitude excitation and the nonlinearity-inducing, higher magnitude excitation is minimized to update the calibration parameters. Thus, model parameter calibration becomes an optimization problem that is solved through an iterative approach combining the multi-harmonic balance method (MHB) and ECRE into a method henceforth referred to as iterative integrated MHB and ECRE (IIME). In this study, the performance and efficiency of IIME are compared against discrete, sampling-based optimal value searches that are commonly used for nonlinear model calibration.

This paper is organized as follows. In Section 2, we briefly review the MHB-ECRE identification approach as applied to nonlinear dynamical systems. Section 3 describes the procedure for the two-step model calibration approach. In Section 4, the calibration approach is demonstrated on the finite element model of an academic example: a nonlinear beam with model error in both the linear and nonlinear components, using synthetically generated measurements. In this section, the efficacy of the proposed two-step approach is evaluated by comparing the obtained results against those of a one-step MHB-ECRE nonlinear model calibration. In Section 5, the limitations of the proposed approach when implemented with reduced quantity (i.e. fewer measured degrees of freedom) and quality (i.e. higher noise levels) of measurements is discussed. Moreover, the effect of the location of the excitation force and model error on the performance of the proposed method is evaluated. Finally, Section 6 draws the conclusions of this paper and summarizes the benefits and drawback of the proposed nonlinear model calibration method compared to the conventional, single-step MHB-ECRE method.

2. Background perspectives: nonlinear model calibration using the MHB-ECRE approach

When calibrating numerical models of dynamical systems, the discrepancy between model predictions and experimental measurements can be calculated using response features in modal, time or frequency domains (Atamturktur *et al.*, 2012). In modal domain, nonlinear effects are projected into modal space in terms of nonlinear normal modes. Nonlinear normal modes are amplitude-dependent, however, which prevents the direct separation of space and time in the governing equations of motion (Vakakis, 1997; Kerschen *et al.*, 2009). This energy dependence complicates the analytical calculation of the nonlinear normal modes, and the model calibration using nonlinear normal models often becomes computationally demanding (Kerschen *et al.*, 2006). The use of time domain response features is less computationally demanding than modal domain features as measurement devices directly provide the desired inputs (Masri and Caughey, 1979; Gondhalekar *et al.*, 2009). Nonetheless, time domain response features are large-dimensional and highly sensitive to measurement noise (Atamturktur and Laman, 2012; Moaveni and Asgarieh, 2012), which makes direct comparisons between the measurements and the model predictions in the time domain highly unreliable.

Frequency domain response features are calculated by applying a transformation process on the time domain signals to separate the response into a series of harmonics (Meyer and Link, 2003; Böswald and Link, 2004). In frequency domain methods, the time and space in the governing equations of motion can be easily separated through linearization using Fourier series expansion. Thus, response features in frequency domain can be expressed as a function of excitation frequency and amplitude (Ferreira and Serpa, 2005). Furthermore, frequency domain features are less sensitive to noise and more compact

compared to the time domain features (Kerschen *et al.*, 2006; Atamturktur and Laman, 2012). In this paper, we implement a class of frequency domain response features known as multi-harmonic coefficients calculated through the MHB method, chosen for their high accuracy (Ren *et al.*, 1998) and computational efficiency (Huang *et al.*, 2006).

2.1 Multi-harmonic balance method

The equation of motion of a nonlinear structure with local geometrical nonlinearity can be written as follows:

$$\boldsymbol{M}\ddot{\boldsymbol{x}}(t) + \boldsymbol{C}\dot{\boldsymbol{x}}(t) + \boldsymbol{K}\boldsymbol{x}(t) + K_{NL}\boldsymbol{x}^3(t) = \boldsymbol{p}(t) \tag{1}$$

where $\boldsymbol{M}, \boldsymbol{C}, \boldsymbol{K} \in \Re^{N,N}$ are the mass, damping and stiffness matrices, respectively, and N is the number of degrees of freedom (DOF) considered. The stiffness matrix is assumed to be positive definite. Here, $\boldsymbol{p}(t)$ is the external force vector and $\boldsymbol{x}(t)$ is the displacement response vector of the N DOFs at time t. In equation (1), a spatially localized, geometrical nonlinearity is represented by the cubic stiffness, K_{NL}, multiplied by the element-wise cube of the displacement of each DOF (Worden and Tomlinson, 2000).

A local, cubic nonlinearity is used in this paper as it is one of the most common cases of nonlinearity in dynamic systems (Kerschen *et al.*, 2006; Wilson *et al.*, 1972). It is important to note, however, the approach presented herein can be used for a wide variety of nonlinear systems (not just local nonlinearities) where the underlying system can be analyzed and calibrated first using intentionally low excitations to the system to isolate the predominately linear behavior of the system (Stricklin and Haisler, 1977).

In linear structural dynamics, the system is conveniently characterized by the structural modes and their associated resonant frequencies. In nonlinear dynamical systems, however, distinctly nonlinear features can be generated from a set of periodic response vectors. When a periodic excitation is applied to a nonlinear dynamical system, the input energy is concentrated at the excitation frequency making it relatively simple to generate nonlinear features through the transformation from time domain response into frequency domain response. This approach also yields higher signal-to-noise ratio compared to the response measured under random or transient excitations (Worden and Tomlinson, 2000). Because of these benefits, solving the equation of motion of a nonlinear system under periodic excitation has become common practice for evaluating the dynamic behavior of nonlinear systems (Kerschen *et al.*, 2006).

Most early approaches for predicting the steady-state oscillation of a nonlinear system under periodic excitation were limited to approximate calculations of the fundamental harmonic coefficients. These fundamental harmonic coefficients were assumed to have a significantly larger value compared to higher order harmonic coefficients (Stoker, 1950; Tondl, 1974). However, in the early 1980s, researchers began to recognize that the higher order harmonic coefficients are also essential to accurately predict the steady state response (Tamura *et al.*, 1981; Leung and Fung, 1989). To include the higher-order harmonics for steady-state oscillations of a nonlinear system, Tamura *et al.* (1981) suggested the MHB method. As an extension of the fundamental harmonic balance approach, MHB operates in the frequency domain to solve nonlinear equations of motion under periodic excitation using a Fourier series approximation. MHB has proven capability solving the periodic response of nonlinear systems more efficiently than time domain integration methods, such as Newmark's, central difference and Runge–Kutta methods (Cardona *et al.*, 1994).

In MHB, the periodic displacement response vector of a nonlinear system is expressed as a Fourier series:

$$\boldsymbol{x}(t) = \boldsymbol{Q}_0 + \sum_{j=1}^{n} \left(\boldsymbol{Q}_j^c \cos m_j \omega t + \boldsymbol{Q}_j^s \sin m_j \omega t \right) \tag{2}$$

where $\boldsymbol{Q}_0$ is a constant; $\boldsymbol{Q}_j^c$ and $\boldsymbol{Q}_j^s$ represent the j^{th} cosine and sine multi-harmonic coefficients, respectively; $m_j$is the harmonic of excitation frequency ω; and n is the number of harmonics included in the analysis. Usually, the multi-harmonic coefficients are obtained by directly applying a fast Fourier transform on the time history response of measured DOFs. If excitation frequency is constant, Fourier series and harmonic curve fitting tools can also be applied for calculating the multi-harmonic coefficients (Isasa *et al.*, 2011).

Introducing equation (2) into the equation of motion for the nonlinear system given in equation (1) results in the following expression:

$$\begin{aligned} &\boldsymbol{M}\left(\sum_{j=1}^{n} \left(-(m_j\omega)^2 \boldsymbol{Q}_j^c \cos m_j \omega t - (m_j\omega)^2 \boldsymbol{Q}_j^s \sin m_j \omega t \right) \right) \\ &+\boldsymbol{C}\left(\sum_{j=1}^{n} \left(-m_j\omega \boldsymbol{Q}_j^c \sin m_j \omega t + m_j\omega \boldsymbol{Q}_j^s \cos m_j \omega t \right) \right) \\ &+\boldsymbol{K}\left(\boldsymbol{Q}_0 + \sum_{j=1}^{n} \left(\boldsymbol{Q}_j^c \cos m_j \omega t + \boldsymbol{Q}_j^s \sin m_j \omega t \right) \right) + K_{NL}\boldsymbol{x}^3(t) = \boldsymbol{p}(t) \end{aligned} \tag{3}$$

Sequentially pre-multiplying all terms in equation (3) by the harmonic functions$(1, \cos m_1\omega t, \sin m_1\omega t \ldots \cos m_n\omega t, \sin m_n\omega t)$ and integrating from zero to the fundamental period of the system, $T = {}^{2\pi}/_{\omega}$, the following frequency domain expression can be obtained (Isasa *et al.*, 2011):

$$\boldsymbol{\mathcal{Z}}(\omega)\boldsymbol{Q}_\omega + \boldsymbol{F}(\boldsymbol{Q}_\omega, \omega) - \boldsymbol{P} = 0 \tag{4}$$

where $\boldsymbol{Q}_\omega = \{Q_0, Q_1, \ldots, Q_{2n}\}$ is the vector of harmonic coefficients with $Q_i \in \Re^{N,1}$. The matrix $\boldsymbol{\mathcal{Z}}(\omega) \in \Re^{(2n+1)N,(2n+1)N}$is a matrix of structural system properties in the frequency domain and is expressed as:

$$\boldsymbol{\mathcal{Z}}(\omega) = \begin{bmatrix} \boldsymbol{K} & 0 & 0 & \ldots & 0 & 0 \\ 0 & \boldsymbol{K} - (m_1\omega)^2\boldsymbol{M} & m_1\omega\boldsymbol{C} & \ldots & 0 & 0 \\ 0 & -m_1\omega\boldsymbol{C} & \boldsymbol{K} - (m_1\omega)^2\boldsymbol{M} & \ldots & 0 & 0 \\ \ldots & \ldots & \ldots & \ldots & \ldots & \ldots \\ 0 & 0 & 0 & \ldots & \boldsymbol{K} - (m_n\omega)^2\boldsymbol{M} & m_n\omega\boldsymbol{C} \\ 0 & 0 & 0 & \ldots & -m_n\omega\boldsymbol{C} & \boldsymbol{K} - (m_n\omega)^2\boldsymbol{M} \end{bmatrix} \tag{5}$$

The nonlinear force vector $K_{NL}\boldsymbol{x}^3(t)$ and periodic excitation force vector $\boldsymbol{p}(t)$ in equation (3) are also transformed from nonlinear, time domain response into linearized, frequency domain response (equation (6) and (7)). It is seen that each harmonic of the periodic excitation yields

corresponding sine and cosine functions not only for the excitation, $\boldsymbol{P}$, but also for the force due to the localized nonlinearity, $\boldsymbol{F}(\boldsymbol{Q}_{\omega}, \omega)$.

Nonlinear force vectors in frequency domain $\boldsymbol{F}(\boldsymbol{Q}_{\omega}, \omega) \in \Re^{(2n+1)N,1}$ are then expressed as:

$$\boldsymbol{F}(\boldsymbol{Q}_{\omega}, \omega) = \left\{ \begin{array}{c} \int_0^T f_{NL}(\boldsymbol{x}(t))dt \\ \frac{\omega}{\pi}\int_0^T f_{NL}(\boldsymbol{x}(t))\cos m_1 \omega t dt \\ \frac{\omega}{\pi}\int_0^T f_{NL}(\boldsymbol{x}(t))\sin m_1 \omega t dt \\ \vdots \\ \frac{\omega}{\pi}\int_0^T f_{NL}(\boldsymbol{x}(t))\cos m_n \omega t dt \\ \frac{\omega}{\pi}\int_0^T f_{NL}(\boldsymbol{x}(t))\sin m_n \omega t dt \end{array} \right\} \text{where} f_{NL}(\boldsymbol{x}(t)) = K_{NL}\boldsymbol{x}^3(t) \tag{6}$$

Periodic excitation force vectors in frequency domain $\boldsymbol{P} \in \Re^{(2n+1)N,1}$ are expressed as:

$$\boldsymbol{P} = \left\{ \begin{array}{c} \int_0^T \boldsymbol{p}(t)dt \\ \frac{\omega}{\pi}\int_0^T \boldsymbol{p}(t) cos m_1 \omega t dt \\ \frac{\omega}{\pi}\int_0^T \boldsymbol{p}(t)\sin m_1 \omega t dt \\ \vdots \\ \frac{\omega}{\pi}\int_0^T \boldsymbol{p}(t)\cos m_n \omega t dt \\ \frac{\omega}{\pi}\int_0^T \boldsymbol{p}(t)\sin m_n \omega t dt \end{array} \right\} \tag{7}$$

Equation (4) can be solved using the Newton–Raphson method (Ferri, 1986). The number of harmonics included must be considered as it increases the size of equation (4), and thus, increases the computation time. Models with prohibitively large linear system matrices can make use of reduction techniques (e.g. Guyan reduction) to reduce computational cost.

2.2 The integrated MHB-ECRE approach

When coupled with the ECRE, a method to measure the element-wise discrepancy between a model and a structure based on constitutive relations, the multi-harmonic coefficients allow the calculation of the residual energy that reflects the discrepancy between predictions and measurements (Charbonnel *et al.*, 2013; Deraemaeker *et al.*, 2002; Hu *et al.*, 2017; Ladevèze and

Leguillon, 1983). By integrating MHB and ECRE, we seek to minimize the constitutive error of the system. This constitutive error, E_ω^2, accounts for the uncertainties in both the model predictions and the experimental measurements and is expressed as:

$$E_\omega^2 = \boldsymbol{r}^T \mathcal{K} \boldsymbol{r}_\omega + \alpha \left(\boldsymbol{H}\boldsymbol{Q}_\omega - \boldsymbol{Q}_\omega^e\right)^T \mathcal{K}_R \left(\boldsymbol{H}\boldsymbol{Q}_\omega - \boldsymbol{Q}_\omega^e\right) \tag{8}$$

where $\mathcal{K} \in \Re^{(2n+1)N,(2n+1)N}$ is the multi-harmonic stiffness matrix (Isasa *et al.*, 2011) and is expressed as:

$$\mathcal{K} = \begin{pmatrix} \boldsymbol{K} & 0 & \cdots & 0 & 0 \\ 0 & \boldsymbol{K} & \cdots & 0 & 0 \\ \vdots & \vdots & \ddots & \vdots & \vdots \\ 0 & 0 & \cdots & \boldsymbol{K} & 0 \\ 0 & 0 & \cdots & 0 & \boldsymbol{K} \end{pmatrix} \tag{9}$$

In equation (8), $\boldsymbol{Q}$ is the multi-harmonic coefficient vector that is expanded from experimentally identified, multi-harmonic coefficients to the total number of DOFs in the numerical model; and $\boldsymbol{Q}_\omega^e$ is the experimentally identified, multi-harmonic coefficient vector that is generated based on the experimentally measured time history response. In this study, only excitation with a constant frequency is considered; hence, $\boldsymbol{Q}_\omega^e$ is obtained using a Fourier series expansion and harmonic curve fitting. In equation (8), $\boldsymbol{r}_\omega = \boldsymbol{Q}_\omega - \boldsymbol{V}_\omega$ is the relative multi-harmonic coefficient vector that accounts for the discrepancy between model predictions and experimental measurements. $\boldsymbol{V}_\omega$ expresses the multi-harmonic coefficients obtained from model predictions. $\boldsymbol{H}$ is a transformation matrix that reduces the multi-harmonic coefficient matrix for all DOFs to the size of the measured DOFs. α is a weighting factor that accounts for the confidence level of experimental measurements (Deraemaeker *et al.*, 2002). Finally, $\mathcal{K}_R$ is the $(2n+1)N_e \times (2n+1)N_e$ reduced multi-harmonic stiffness matrix of the numerical model obtained through Guyan model reduction (Guyan, 1965), where N_e is the number of measured DOFs.

To evaluate $\boldsymbol{r}_\omega$ and $\boldsymbol{Q}$, we solve the following minimization problem:

Minimize cost function:

$$E_\omega^2 = \boldsymbol{r}^T \mathcal{K} \boldsymbol{r}_\omega + \alpha \left(\boldsymbol{H}\boldsymbol{Q}_\omega - \boldsymbol{Q}_\omega^e\right)^T \mathcal{K}_R \left(\boldsymbol{H}\boldsymbol{Q}_\omega - \boldsymbol{Q}_\omega^e\right) \tag{10a}$$

Subjected to constraint relationship:

$$\mathcal{Z}(\omega)\boldsymbol{Q}_\omega + \boldsymbol{F}(\boldsymbol{Q}_\omega, \omega) - \boldsymbol{P} = \mathcal{K}\boldsymbol{r}_\omega \tag{10b}$$

The constraint in equation (10b) can be dualized using a Lagrange multiplier to form an unconstrained minimization problem.

3. Calibrating the models of nonlinear dynamical systems: iterative integrated MHB and ECRE (IIME)

The two-step process presented herein is conceived to identify the residual errors in the underlying linear system and those in the nonlinear component. The strategy implemented involves measuring the dynamical system vibration response under low magnitude periodic excitation such that the system vibration response is predominantly linear. Using this low magnitude excitation ($\boldsymbol{P}_1$) data, the experimental multi-harmonic coefficients ($\boldsymbol{Q}_{\omega 1}^e$) are first obtained. Next, model-predicted multi-harmonic coefficients ($\boldsymbol{V}_{\omega 1}$) are calculated and

experimental multi-harmonic coefficients ($\boldsymbol{Q}_{\omega 1}$) are expanded to match the degrees of freedom of the numerical model. Through the error minimization step of ECRE, the difference between experimental multi-harmonic coefficient and model predicted multi-harmonic coefficient vectors ($\boldsymbol{Q}_{\omega 1} - \boldsymbol{V}_{\omega 1}$) is calculated. The knowledge of this disagreement, combined with the stiffness matrix, allows us to calculate the elemental residual energy. The elements with high residual energy indicate the existence of higher model error (Hu *et al.*, 2017), and thus, the model parameters associated with these elements are selected for calibration. This model error localization step is useful for parameter selection (Larsson and Abrahamsson, 1999; Kim and Park, 2004; Hu *et al.*, 2017) because the number of parameters that need to be calibrated can often be significantly reduced in this step, which in turn helps mitigate the risk of rank deficiency and ill-conditioning during calibration (Yu *et al.*, 2007).

In the second step, a higher magnitude periodic excitation is applied to obtain the nonlinear dynamic displacement response and the corresponding multi-harmonic coefficient is calculated ($\boldsymbol{Q}^{e}_{\omega 2}$). Using both multi-harmonic coefficients, $\boldsymbol{Q}_{\omega 1}$ and $\boldsymbol{Q}_{\omega 2}$, linear and nonlinear model parameters are calibrated by minimizing the sum of the residual energy calculated for both excitation magnitudes ($\boldsymbol{P}_1$ and $\boldsymbol{P}_2$). This way the model error in the locally nonlinear component is accurately identified all while errors in the modeling of the underlying linear system are corrected. Figure 1 schematically shows the proposed method as divided into two steps: localization and parameter calibration. The details of these two steps are given below:

Step 1. Model error localization using low magnitude excitation, $\boldsymbol{P}_1$.

Based on the system response to low magnitude excitation, the optimization problem is formulated in equation (11) that minimizes the residual energy between the numerical model and the measurements. To minimize the objective function, we formulate a saddle-point problem with the introduction of Lagrange multipliers. equation (11) yields the system of the nonlinear equations shown in equation (12), based on which the two unknown multi-harmonic coefficient vectors, $\boldsymbol{r}_{\omega 1}$ and $\boldsymbol{Q}_{\omega 1}$, that represent the predominantly linear dynamic response features can be solved. The relative multi-harmonic coefficient vector $\boldsymbol{r}_{\omega 1}$, combined with elemental stiffness matrix, is then used for localizing the model error in the linear component. Therefore, the linear parameters that are associated with identified model error, E_L, are selected from a large candidate set of parameters for the calibration in the next step.

Minimize the cost function for force level $\boldsymbol{P}_1$:

$$E^2_{\omega 1} = \boldsymbol{r}_1^T \mathcal{K}^{\omega 1} \boldsymbol{r}_{\omega 1} + \alpha \left(\boldsymbol{H}\boldsymbol{Q}_{\omega 1} - \boldsymbol{Q}^{e}_{\omega 1}\right)^T \mathcal{K}_R \left(\boldsymbol{H}\boldsymbol{Q}_{\omega 1} - \boldsymbol{Q}^{e}_{\omega 1}\right) \tag{11a}$$

Subjected to constraint relationship:

$$\mathcal{Z}(\omega)\boldsymbol{Q}_{\omega 1} + F(\boldsymbol{Q}_{\omega 1}, \omega, K_{NL}) - \boldsymbol{P}_1 = \mathcal{K}\boldsymbol{r}_{\omega 1} \tag{11b}$$

Nonlinear matrix equation:

$$\begin{pmatrix} \mathcal{Z}(\omega) + \dfrac{\partial \boldsymbol{F}(\boldsymbol{Q}_{\omega 1}, \omega, K_{NL})}{\partial \boldsymbol{Q}_{\omega 1}} & \alpha \boldsymbol{H}^T \mathcal{K}_R \boldsymbol{H} \\ \mathcal{K} & -\mathcal{Z}(\omega) \end{pmatrix} \begin{Bmatrix} \boldsymbol{r}_{\omega 1} \\ \boldsymbol{Q}_{\omega 1} \end{Bmatrix} + \begin{Bmatrix} 0 \\ -\boldsymbol{F}(\boldsymbol{Q}_{\omega 1}, \omega, K_{NL}) \end{Bmatrix} = \begin{Bmatrix} \alpha \boldsymbol{H}^T \mathcal{K}_R \boldsymbol{Q}^{e}_{\omega 1} \\ -\boldsymbol{P}_1 \end{Bmatrix} \tag{12}$$

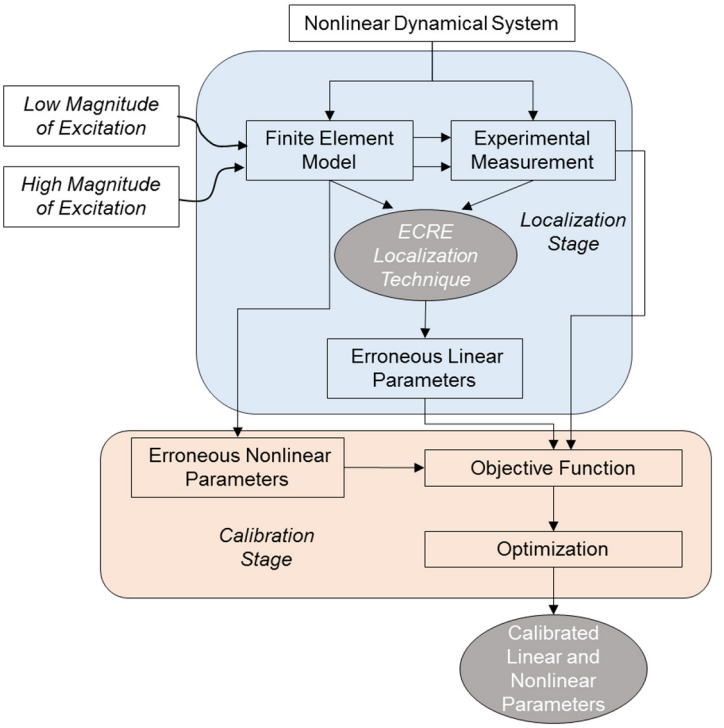

Figure 1.
The calibration procedure for the proposed method

The derivation of equation (12) can be found by considering equation (11a) as a saddle-point problem and applying Lagrange multipliers. The terms that compose equation (11a) are classified as being "less reliable," namely, the error in the model (first term) and the mode shape expansion error (second term) that is introduced when the experimentally measured information is extrapolated to the N model DOFs (Zimmerman and Kaouk, 1994; Charbonnel *et al.*, 2013). By subsequently applying the constraint to the optimization problem that the solution must satisfy the more reliable equilibrium equation of equation (11b), the errors in less reliable equations can be minimized.

Step 2. Nonlinear model calibration using both low and high magnitude excitations, P1 and P2.

In the second step, we combine the measurements of multi-harmonic coefficients for both low and high magnitude excitations. The sum of the residual energy for both excitation magnitudes is then minimized.

Minimize the cost function for $\boldsymbol{P}_1$ and $\boldsymbol{P}_2$:

$$E^2_{\omega\_combined} = \boldsymbol{r}_{\omega 1}^T \boldsymbol{\mathcal{K}} \boldsymbol{r}_{\omega 1} + \alpha\left(\boldsymbol{H}\boldsymbol{Q}_{\omega 1} - \boldsymbol{Q}^{\ell}_{\omega 1}\right)^T \boldsymbol{\mathcal{K}}_R \left(\boldsymbol{H}\boldsymbol{Q}_{\omega 1} - \boldsymbol{Q}^{\ell}_{\omega 1}\right) + \boldsymbol{r}_{\omega 2}^T \boldsymbol{\mathcal{K}} \boldsymbol{r}_{\omega 2} + \alpha\left(\boldsymbol{H}\boldsymbol{Q}_{\omega 2} - \boldsymbol{Q}^{\ell}_{\omega 2}\right)^T \boldsymbol{\mathcal{K}}_R \left(\boldsymbol{H}\boldsymbol{Q}_{\omega 2} - \boldsymbol{Q}^{\ell}_{\omega 2}\right) \tag{13a}$$

Subjected to the following constraints:

$$\boldsymbol{\mathcal{Z}}(\omega)\boldsymbol{Q}_{\omega 1} + \boldsymbol{F}(\boldsymbol{Q}_{\omega 1}, \omega, K_{NL}) - \boldsymbol{P}_1 = \boldsymbol{\mathcal{K}}\boldsymbol{r}_{\omega 1} \tag{13b}$$

$$\boldsymbol{\mathcal{Z}}(\omega)\boldsymbol{Q}_{\omega 2} + \boldsymbol{F}(\boldsymbol{Q}_{\omega 2}, \omega, K_{NL}) - \boldsymbol{P}_2 = \boldsymbol{\mathcal{K}}\boldsymbol{r}_{\omega 2} \tag{13c}$$

A new cost function g_c is obtained after applying the Lagrange multipliers and is expressed as follows:

$$\begin{aligned} g_c = {} & \boldsymbol{r}_1^T \boldsymbol{\mathcal{K}}^{\omega 1} \boldsymbol{r}_{\omega 1} + \alpha\left(\boldsymbol{H}\boldsymbol{Q}_{\omega 1} - \boldsymbol{Q}^e_{\omega 1}\right)^T \boldsymbol{\mathcal{K}}_R \left(\boldsymbol{H}\boldsymbol{Q}_{\omega 1} - \boldsymbol{Q}^e_{\omega 1}\right) \\ & + {\psi_1}^T \left(\boldsymbol{\mathcal{K}}\boldsymbol{r}_{\omega 1} - \boldsymbol{\mathcal{Z}}(\omega)\boldsymbol{Q}_{\omega 1} - \boldsymbol{F}(\boldsymbol{Q}_{\omega 1}, \omega, K_{NL}) + \boldsymbol{P}_1\right) \\ & + \boldsymbol{r}_2^T \boldsymbol{\mathcal{K}}^{\omega 2} \boldsymbol{r}_{\omega 2} + \alpha\left(\boldsymbol{H}\boldsymbol{Q}_{\omega 2} - \boldsymbol{Q}^e_{\omega 2}\right)^T \boldsymbol{\mathcal{K}}_R \left(\boldsymbol{H}\boldsymbol{Q}_{\omega 2} - \boldsymbol{Q}^e_{\omega 2}\right) \\ & + {\psi_2}^T \left(\boldsymbol{\mathcal{K}}\boldsymbol{r}_{\omega 2} - \boldsymbol{\mathcal{Z}}(\omega)\boldsymbol{Q}_{\omega 2} - \boldsymbol{F}(\boldsymbol{Q}_{\omega 2}, \omega, K_{NL}) + \boldsymbol{P}_2\right) \end{aligned} \tag{14}$$

where ψ_1 and $\psi_2$are the Lagrange multipliers for the constraint relationships for $\boldsymbol{P}_1$ and $\boldsymbol{P}_2$, respectively. Through the calculation of the stationary conditions of g_c with respect to the unknowns $\boldsymbol{r}_{\omega 1}$, $\boldsymbol{Q}_{\omega 1}$, $\boldsymbol{r}_{\omega 2}$, $\boldsymbol{Q}_{\omega 2}$, E_L, K_{NL}, ψ_1, and ψ_2, the solution of equation (14) is calculated using the following matrix relationship:

$$\begin{bmatrix} \boldsymbol{\mathcal{Z}}(\omega) + \dfrac{\partial \boldsymbol{F}(\boldsymbol{Q}_{\omega 1}, \omega, K_{NL})}{\partial \boldsymbol{Q}_{\omega 1}} & \alpha \boldsymbol{H}^T \boldsymbol{\mathcal{K}}_R \boldsymbol{H} & 0 & 0 & 0 & 0 \\ \boldsymbol{\mathcal{K}} & -\boldsymbol{\mathcal{Z}}(\omega) & 0 & 0 & 0 & 0 \\ 0 & 0 & \boldsymbol{\mathcal{Z}}(\omega) + \dfrac{\partial \boldsymbol{F}(\boldsymbol{Q}_{\omega 2}, \omega, K_{NL})}{\partial \boldsymbol{Q}_{\omega 2}} & \alpha \boldsymbol{H}^T \boldsymbol{\mathcal{K}}_R \boldsymbol{H} & 0 & 0 \\ 0 & 0 & \boldsymbol{\mathcal{K}} & -\boldsymbol{\mathcal{Z}}(\omega) & 0 & 0 \\ 0 & 0 & 0 & 0 & 0 & 0 \\ 0 & 0 & 0 & 0 & 0 & 0 \end{bmatrix} \begin{Bmatrix} \boldsymbol{r}_{\omega 1} \\ \boldsymbol{Q}_{\omega 1} \\ \boldsymbol{r}_{\omega 2} \\ \boldsymbol{Q}_{\omega 2} \\ E_L \\ K_{NL} \end{Bmatrix} + \begin{Bmatrix} 0 \\ -\boldsymbol{F}(\boldsymbol{Q}_{\omega 1}, \omega, K_{NL}) \\ 0 \\ -\boldsymbol{F}(\boldsymbol{Q}_{\omega 2}, \omega, K_{NL}) \\ \dfrac{\partial g}{\partial E_L} \\ \dfrac{\partial g}{\partial K_{NL}} \end{Bmatrix} = \begin{Bmatrix} \alpha \boldsymbol{H}^T \boldsymbol{\mathcal{K}}_R \boldsymbol{Q}^e_{\omega 1} \\ -\boldsymbol{P}_1 \\ \alpha \boldsymbol{H}^T \boldsymbol{\mathcal{K}}_R \boldsymbol{Q}^e_{\omega 2} \\ -\boldsymbol{P}_2 \\ 0 \\ 0 \end{Bmatrix} \tag{15}$$

where E_L are the linear structural parameters corresponding to the identified model error in the linear component.

All the above objective functions are convex, thus facilitating the use of efficient local optimization algorithms in the calibration process. A modified Newton–Raphson algorithm is chosen to solve this nonlinear problem due to its desirable convergence characteristics (Nocedal and Wright, 2006; Stevens *et al.*, 2017) and because the parameter gradients are calculated numerically. In each of the Newton–Raphson iterations, the parameters are calibrated and the residual error term is recalculated. A new iteration consisting of a

localization step, and a correction step is performed until the prescribed convergence criterion is satisfied.

Instead of iteratively calibrating the parameters corresponding to linear and nonlinear behavior (i.e. using IIME), calibration can also be conducted based on a discrete set of inputs—henceforth referred to as discrete integrated MHB-ECRE (DIME). In the DIME approach, a sample set of values are generated for the poorly known model input parameters and then used for calculation of the residual energy using equation (13) and (14). As such, the minimum residual energy is expected to be achieved when the calibration parameters associated with the linear and nonlinear components are closest to the true parameter values. In DIME, a large number of instances must be calculated, which means the discrete approach is more computationally demanding than IIME. In the following section, the results obtained with the DIME approach are used as a reference to compare against those obtained with the proposed two-step IIME approach.

4. Benchmark beam model application

4.1 The description of the numerical model

The proposed approach is demonstrated on a simulated academic example based on the COST action F3 project benchmark structure developed at Ecole Centrale de Lyon (Thouverez, 2003; Worden, 2003). The model consists of a main beam clamped to a thin, secondary beam with both ends of the structure clamped to fixed supports (Figure 2). The main beam has a length of 0.7 m and a thickness of 0.014 m, whereas the secondary beam has a length of 0.04 m with a thickness of 5×10^{-4} m. Both beams have a width of 0.014 m and comprise steel with a Young's modulus of 210 GPa and a Poisson's ratio of 0.33. Table I lists the reference configuration of the F3 project benchmark model. The main beam is modeled with seven elements and the secondary beam with four elements as shown in Figure 2. The connection of the beams is modeled by a semi-rigid, rotational spring and a grounded, translational spring element with cubic stiffness such that the nodes are constrained to have the same translation displacement, but allowed to have different rotations. The value of the cubic stiffness (K_{NL}) is set to be 6.1×10^9 N/m.

Vibration response measurements are synthetically generated for 21 DOFs along the beam as shown in Figure 3. For the low magnitude excitation, a stepped sine force with a magnitude of 0.5 N and frequency of 32 Hz, selected based on the value of the fundamental frequency of the linear beam, is applied to the structure. For the high magnitude excitation, a stepped sine force with a magnitude of 5 N and frequency of 32 Hz is applied to ensure sufficiently large deflections to observe the nonlinear dynamic effects. In addition, simulated measurement noise is introduced as an additive zero mean Gaussian white noise at a level of 5 per cent of the maximum displacement time history response. The noise is added to the

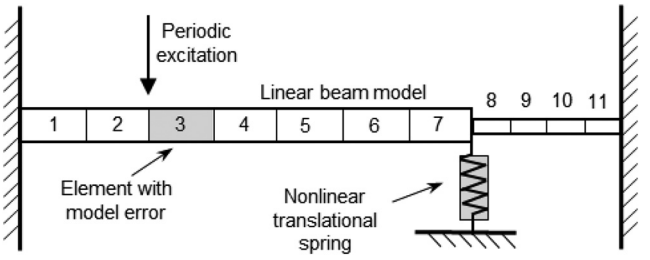

Figure 2.
A linear beam model with local nonlinearity under periodic excitation

Symbol	Parameter	Value
L_1	Length of main beam	0.7 m
L_2	Length of thin beam	0.04 m
b	Width of cross section	0.14 m
h_1	Height of main beam	0.14 m
h_2	Height of thin beam	0.0005 m
ρ	Density	7830 kg/m^3
E	Young's modulus	210 GPa
ν	Poisson's ratio	0.33
N_{node}	Node number	12
N_{dof}	DOF number	21
N_e	Beam element number	11
N_m	Measured DOFs	21

Table I. Reference configuration of the benchmark beam model

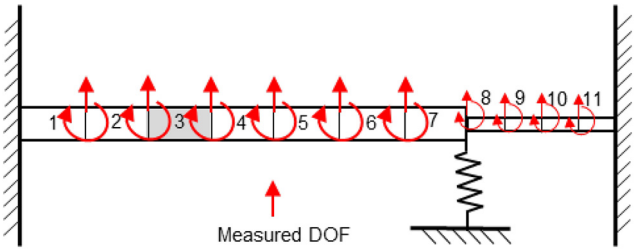

Figure 3. The experimentally measured translational and rotational DOFs

time history measurements before the experimental multi-harmonic coefficients vectors are calculated.

The initial model is preset to have error in two distinct forms (recall Figure 2): model error in the linear beam structure that is simulated by intentionally reducing the Young's modulus for element 3 by 50 per cent (i.e. 105 GPa); model error in the nonlinear spring that is simulated by intentionally altering the stiffness coefficient with cubic nonlinearity by 50 per cent (i.e. 3.05×10^9 N/m).

4.2 The conventional approach: MHB-ECRE using only high magnitude excitation

This section presents the results of the conventional, one-step MHB-ECRE approach in which the parameter of the nonlinear translational stiffness (K_{NL}) is calibrated with the presumption that the model of the underlying linear system is error-free. The effect of the model error in the linear beam on the results of this conventional approach is evaluated using both a model with and without the manually introduced reduction in the Young's modulus of element 3.

Owing to the need that the structure's dynamic response must exhibit nonlinear behavior for the one-step MHB-ECRE method, synthetic response measurements are generated by the model under the high amplitude excitation (5 N), using which the ECRE values are calculated by solving equation (11).

Figure 4 depicts the ECRE values obtained for a range of nonlinear stiffness values where the correction coefficient that multiplies the nonlinear stiffness parameter (K_{NL}) varies from 0.5 to 1.5 with an interval of 0.1, essentially representing a correction of 50 per cent below and above the nominal stiffness value. For this given range of nonlinear

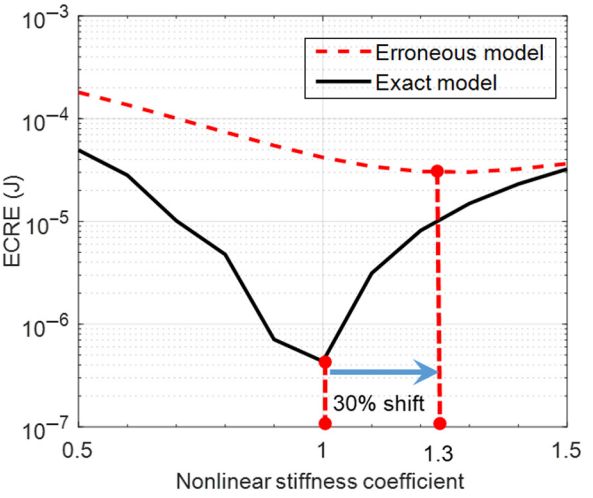

Figure 4.
Nonlinear parameter identification result when the linear stiffness coefficient is 0.5 and 1

stiffness coefficients, the residual energy is calculated using both the "exact" linear model (the solid curve in Figure 4) and the "erroneous" linear model (i.e. one with a reduced Young's modulus in element 3; the dashed curve in Figure 4). The results shown in Figure 4 indicate that the linear model error leads to a 30 per cent deviation from the true value for the identified nonlinear stiffness parameter. This difference is due to the fact that the ECRE values are biased by the model error present in the linear component and thus, the minima no longer corresponds to the *true* value of the nonlinear stiffness.

4.3 The two-step approach: MHB-ECRE using two excitation magnitudes

In this section, the proposed, iterative, two-step approach is used to calibrate the model input parameters of both the Young's modulus of element 3 and the nonlinear stiffness (K_{NL}) and verify its ability to accurately calibrate the parameters without suffering the confounding effects of error in both the linear and nonlinear components of the structure. The efficiency of this iterative approach in its search algorithm to find the optimal input parameters is compared to the discrete (DIME) approach which tests over a grid sampling of possible parameters.

The structure is excited at Node 3 using the lower amplitude periodic force (0.5 N) to obtain the synthetic structural vibration response with negligible nonlinear effects. As shown in Figure 5(a), the nonlinear effects lead to only a 1.5 per cent shift in the fundamental frequency of the structural system, while no significant distortion can be observed in the frequency response function (FRF) of the nonlinear beam model with respect to the linear model. Hence, the obtained dynamic response is predominantly linear. The ECRE calculated for all beam elements is shown in Figure 6. From the figure, Element 3 (E_L) is identified with the highest ECRE value, which is consistent with the fact that an incorrect Young's modulus value is assigned for this element.

The structure is then excited at the same location using the higher amplitude periodic excitation (5N) to observe the synthetic nonlinear vibration. The FRF of the translational DOF associated with the nonlinear spring is presented in Figure 5(b). A significant distortion of 12.5 per cent in the FRF plots is observed where the peaks shift from 32 to 36 Hz under high magnitude excitation, confirming that a sufficiently high force is applied to observe the nonlinear response.

Both IIME and DIME approaches are used to calibrate the selected model parameters as presented in the Figure 7. The IIME approach is applied by solving equation (15) using the Newton–Raphson algorithm. The convergence threshold for the IIME approach is set to 10^{-10} for the norm of the relative solution vector between iterations. In Figure 7, it is noticed that the IIME approach is completed within 5 iterations. The calibrated linear and nonlinear model parameters are 210.21 GPa and 6.08×10^9 N/m, respectively, which represent a 0.1 and 0.4 per cent deviation from the true values, respectively. The detailed calibration results for each iteration are also provided in Table II. For the DIME approach, a range of coefficients that multiply the nonlinear stiffness (K_{NL}) and Young's modulus in the linear component (E_L) is created from 50 to 150 per cent of the true value with an interval of 10 per cent. These pre-defined sets of model parameters are substituted into equation (15) and a surface plot of the residual energy is shown in Figure 7. The detailed calibration results for each iteration are also provided in Table II.

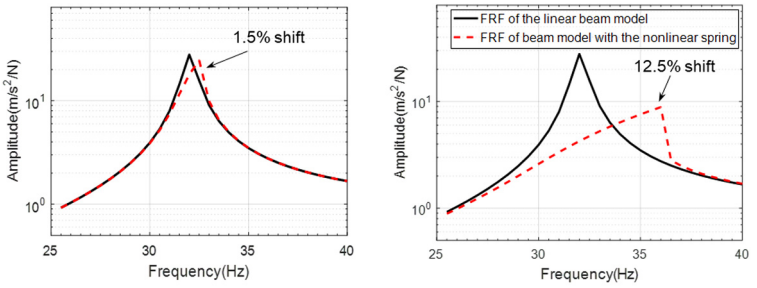

(a) (b)

Notes: (a) A low magnitude excitation of 0.5 N is applied; (b) a high magnitude excitation of 5 N is applied

Figure 5. Comparison of FRFs at node 8 for the linear beam model with and without the nonlinear spring

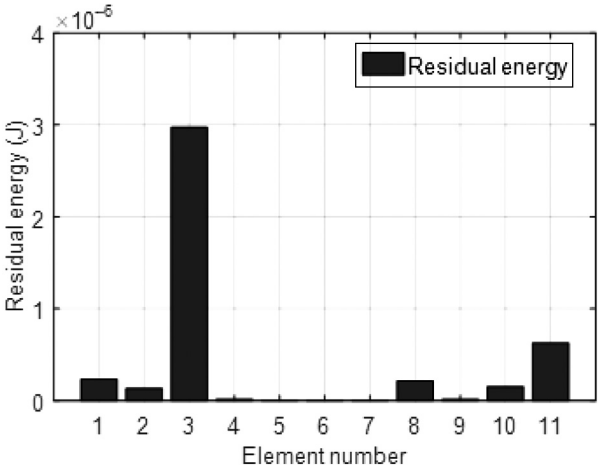

Figure 6. The ECRE localization of model error in linear component

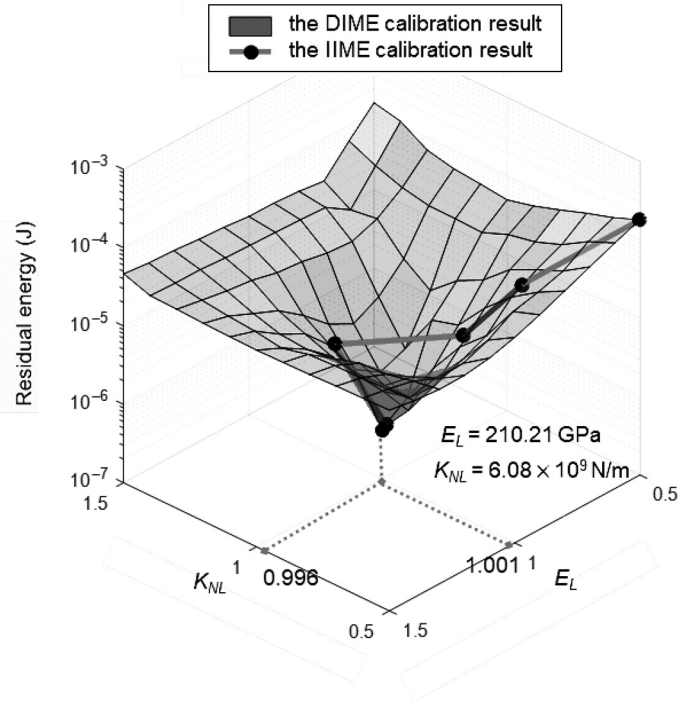

Figure 7.
The calibration result for the linear and nonlinear parameters

Iteration no.	Calibrated linear parameter (GPa)	(%) error	Calibrated nonlinear parameter (*N/m*)	(%) error	ECRE
0	105	−50.00	3.05×10^9	−50.00	1.81×10^{-5}
1	159.18	−24.20	4.28×10^9	−29.80	3.50×10^{-5}
2	182.28	−13.20	4.98×10^9	−18.30	7.91×10^{-6}
3	223.86	6.60	6.80×10^9	11.50	4.40×10^{-6}
4	210.21	0.10	5.99×10^9	−1.80	5.18×10^{-7}
5	210.21	0.10	6.08×10^9	−0.40	4.34×10^{-7}

Table II.
Model calibration results using IIME approach

5. Discussions on the performance of proposed method

In this section, the impact of measurement noise, number of response measurement locations, and model error location on the accuracy of the proposed method is examined. The purpose of conducting these studies is to evaluate the proposed approach's robustness and to understand how the method performs under a variety of realistic scenarios. All the calibration results presented in this section are obtained using an identical procedure as detailed in Section 4.

5.1 Model calibration considering varying noise levels

All practical experimental data is inevitably contaminated by noise to some degree (Modak *et al.*, 2002). To assess the impact of measurement noise, in this section, the performance of

the proposed model calibration method is evaluated in the presence of varying levels of noise. Accordingly, the two-step model calibration process is applied in the presence of zero mean Gaussian white noise with varying standard deviations of 5, 10, 15 and 20 per cent. For each noise level, ten random realizations of noise are generated to contaminate the time history data and the calibrated model parameters are obtained using these contaminated measurements.

The mean and standard deviation for the calibrated stiffness coefficients for these ten realizations are shown in Figure 8. The solid line in Figure 8 shows that the linear stiffness parameter is estimated with less than 1 per cent deviation from the true value when the noise level is less than 15 per cent. With 20 per cent noise, the calibrated linear stiffness parameter deviates by 5.6 per cent. The calibrated nonlinear stiffness parameter is observed to be more sensitive to the measurement noise. The dashed line in Figure 8 shows that the nonlinear stiffness parameter is accurately estimated with less than 1 per cent deviation when the noise level is less than 10 per cent. As the noise level increases to 15 and 20 per cent, the calibrated nonlinear stiffness parameter deviates by 6.1 and 11.2 per cent, respectively.

5.2 Model calibration with reduced set of measurements

In practical application, the number of measured response locations is limited by the feasible number of sensors, measurement channels available and the inaccessibility of some measurement locations (Majumder and Manohar, 2003). To assess the effect of such limitations, this section evaluates he performance of the proposed two-step model calibration approach by hypothetically reducing the set of measured DOFs. Three reduced sets of measurements are used to obtain the multi-harmonic coefficient vectors as shown in Figure 9. The first two measurements are with 10 (Figure 9 (a) and 5 (Figure 9 (b)

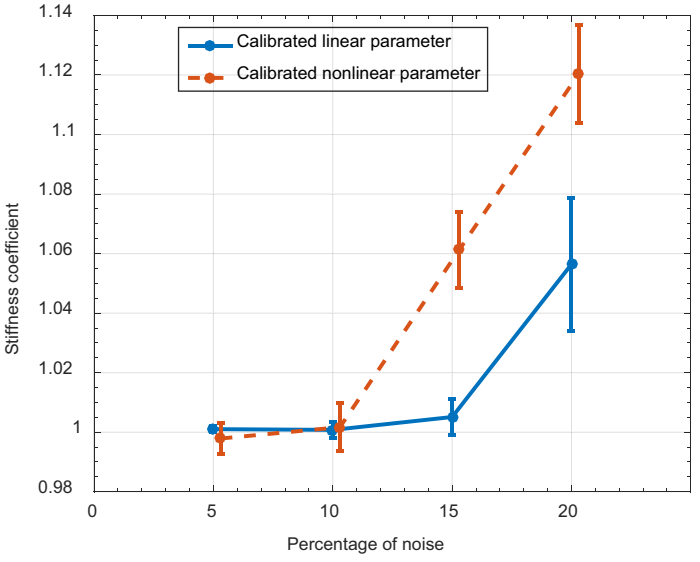

Note: The true values of both parameters correspond to a stiffness coefficient value of 1

Figure 8.
Mean and standard deviation error bars illustrating the calculated value of the calibrated linear and nonlinear stiffness parameters under a variety of noise levels using the proposed approach

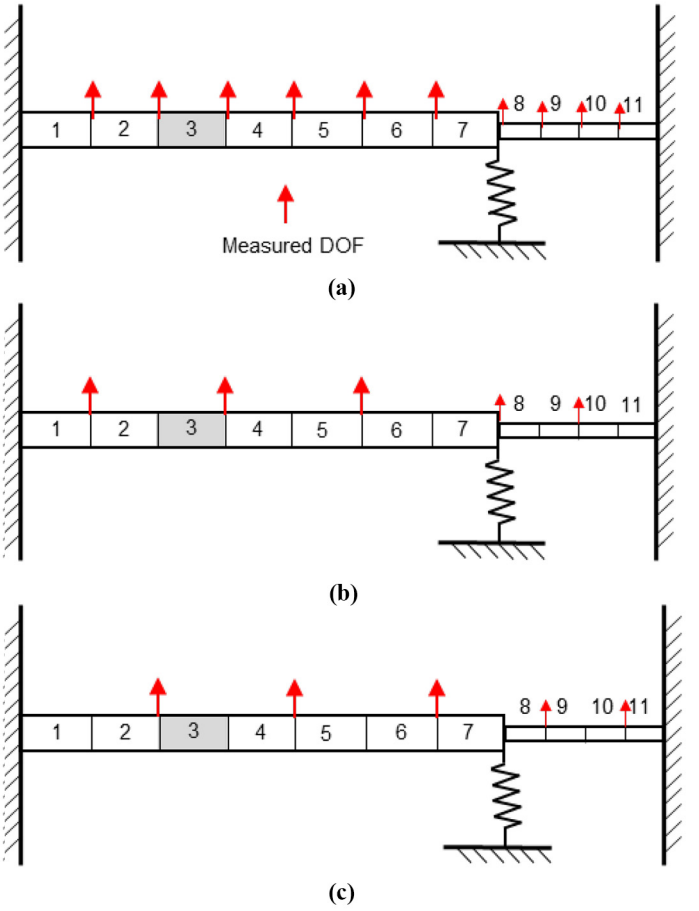

Figure 9.
Three sets of reduced DOF measurements

Notes: (a) Measurement with 10 DOFS; (b) measurement with 5 DOFs including the local nonlinear DOF; (c) measurement with 5 DOFs not including the local nonlinear DOF

translational DOFs including the DOF at the nonlinear spring, while the last set of measurements is with 5 (Figure 9 (c)) translational DOFs excluding the DOF at the nonlinear component. Using the reduced set of measurements, the residual energy plot for model error localization is shown in Figure 10.

As seen in Figure 11, the calibrated values for the nonlinear stiffness coefficient match the true parameter values even when the number of measurements is as low as 5 DOFs. The value of the parameter associated with the linear element with error is correctly calibrated with 10 measured DOFs, while an 8 per cent deviation from the true values is present when only 5 DOFs are measured. When the DOF at the nonlinear spring is not included in the measurement, Figure 12 shows that the linear calibrated stiffness coefficient has a 12.3 per cent deviation from the true value, and the nonlinear

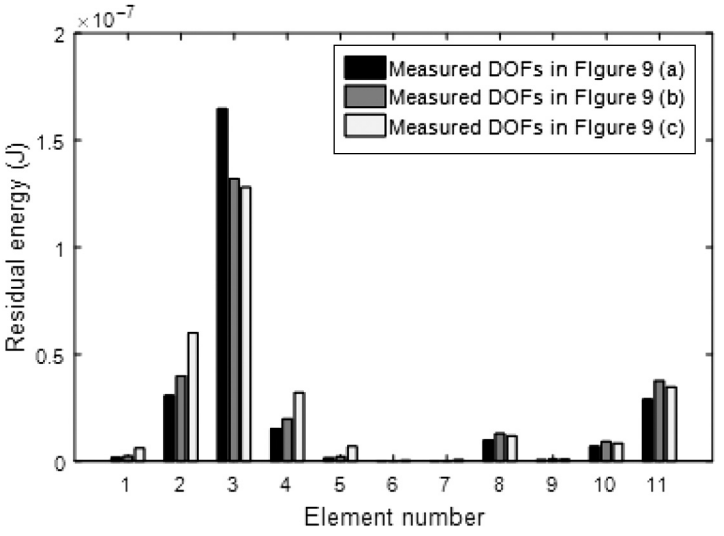

Figure 10.
The ECRE localization of linear model error using reduced sets of measurements

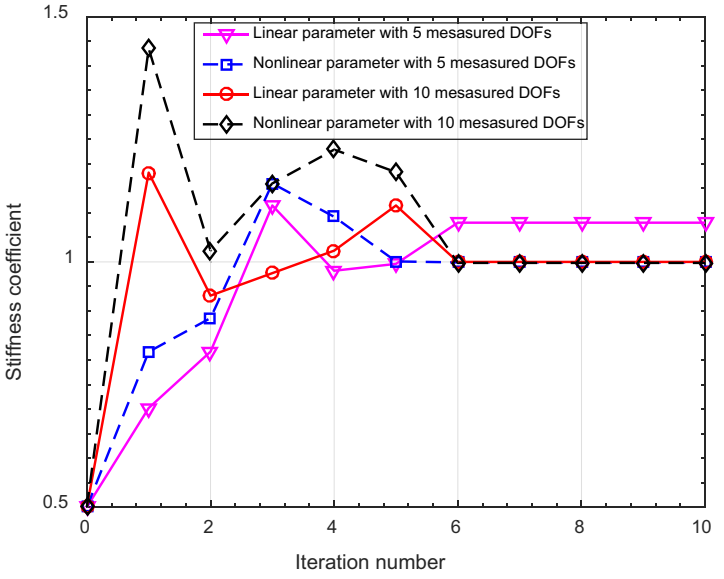

Figure 11.
Calibration results with fewer measured DOFs (the nonlinear DOF is included)

calibrated stiffness coefficient has a 26.1 per cent deviation from the true value. The calibration of the nonlinear stiffness coefficient parameter is less affected by a reduced set of measurements as long as the response associated with the nonlinear spring is measured. It is concluded that it is important to measure the response as close to where local nonlinearity is present as possible to ensure the accuracy of the results of the proposed model calibration method.

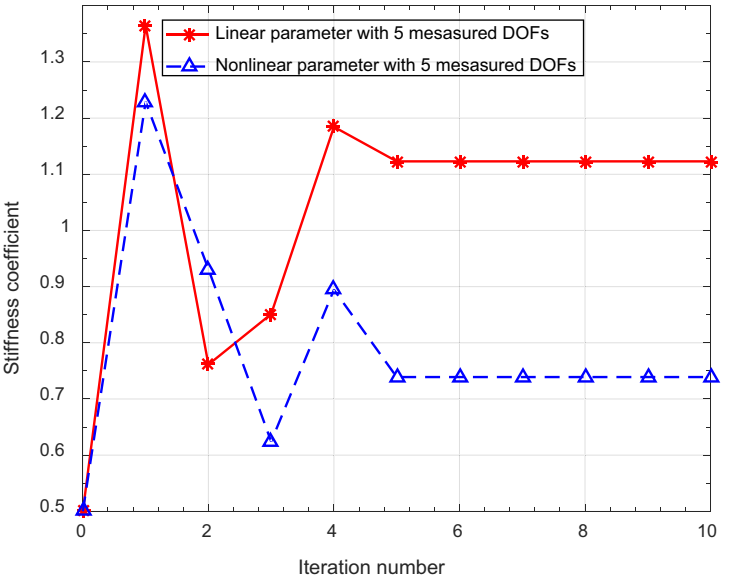

Figure 12.
Calibration results with five measured DOFs (not including the nonlinear DOF)

5.3 The effect of model error location

The objective of this section is to investigate the effect the spatial distribution of modeling error on the linear system on the obtained results for the calibrated model. Specifically, we introduced model error to 7 different elements (elements 1 to 7) of the main beam, simulated by reducing the Young's modulus by 50 per cent. The model error in the nonlinear component is kept the same as defined in Section 4 for the seven sets of calibration cases. The proposed approach is applied to calibrate the linear and nonlinear structural component parameters, and the calibration results are plotted in Figure 13(a) and (b), respectively. As shown in the Figure 13(a) and (b), the convergence rate to the true value for the linear and nonlinear stiffness parameters is similar (five iterations) for all seven cases regardless of the model error location.

5.4 The effect of excitation force location

In this section, the effect of the location of the excitation force, and thus the distance between the applied force location and nonlinear spring component on the performance of model calibration results is evaluated (Figure 14). Similar to the calibration results presented in Section 5.3, the unknown structural parameters mostly converge to the true value with the proposed calibration approach. The calibration results for all seven force locations are presented in Figure 13(c) and (d). Figure 13(c) shows that the averaged calibrated nonlinear stiffness coefficient relative to the true value for different locations is 0.9992 with a standard deviation of 0.0029.

Compared to the calibration of the nonlinear structural parameter, the average calibrated linear stiffness coefficient is 1.0232, which deviates slightly from the true parameter value (Figure 13 (d)). Also, a larger standard deviation of 0.0362 is observed relative to the nonlinear stiffness calibration. Moreover, it can be concluded from Figure 13(b) and (d) that the calibration of linear model parameters is affected by the

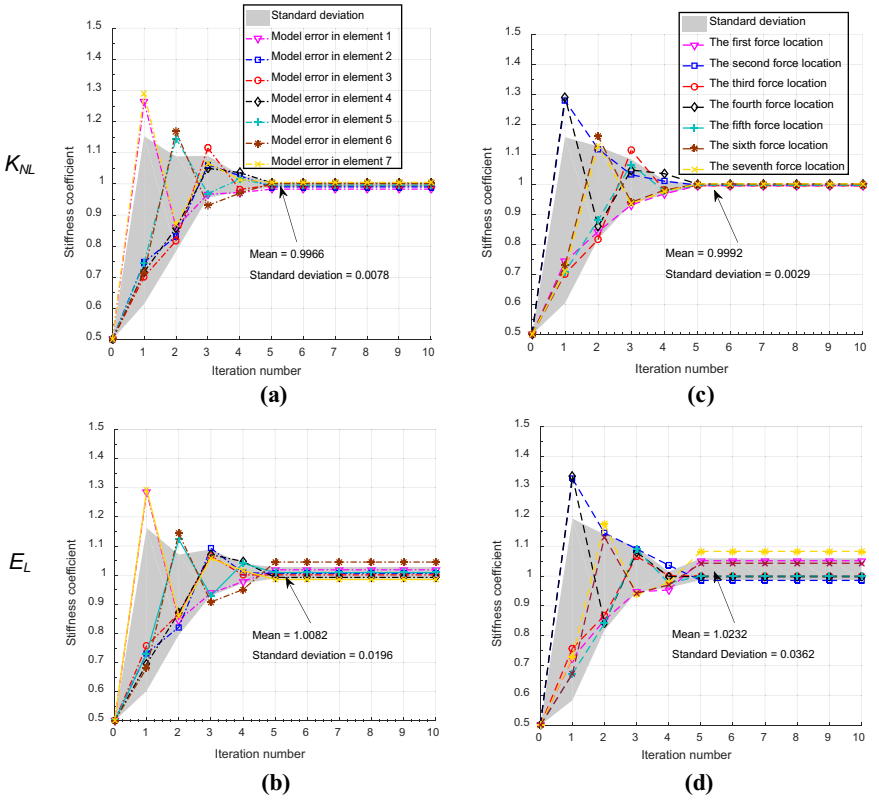

Figure 13.
Calibration results considering the effect of model error location and excitation force location

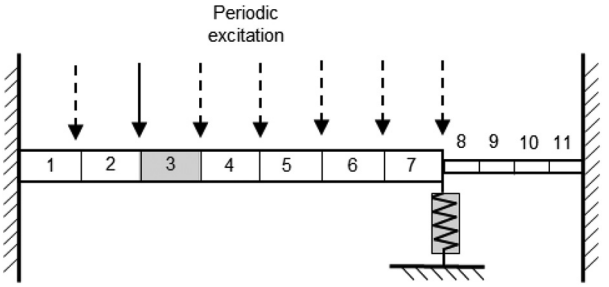

Figure 14.
Seven locations for applied excitation force

location of the excitation force relative to the location of the model error. As the excitation force moves from the left end of the beam to the right end, the calibrated linear parameters deviate more from the true parameter value. This effect may be because as the magnitude of response becomes larger as the distance between force location and nonlinear spring element decreases, the total response is more likely to be dominated by the nonlinear effect. Thus, the accuracy of the linear parameter calibration results is influenced.

6. Conclusion

This paper presents a two-step, nonlinear model calibration framework referred to as IIME that simultaneously corrects modeling error in both linear and nonlinear components based on the combined MHB-ECRE algorithm. An appealing feature of this approach is that modeling errors in the underlying linear model can be isolated and corrected, reducing their degrading effects in the model calibration of the nonlinear component. For this, the modeling errors in the linear system are localized by applying low magnitude excitation that ensures the dynamic response of the system remains predominantly linear. Accordingly, subsequent optimization step for parameter calibration is formulated to determine both the parameters associated with poorly modeled linear components and those associated with the nonlinear components without making any assumptions regarding initial linear model accuracy.

The proposed method has been demonstrated on a numerical example (the F3 project benchmark structure) using synthetic measurements. The results show that the Integrated MHB-ECRE method is capable of calibrating nonlinear models with model error in both linear and nonlinear components. When model error is present in both linear and nonlinear components, this two-step integrated MHB-ECRE calibration approach has shown superiority to the conventional one-step MHB-ECRE approach of previous literature, while providing more reliable calibration of the nonlinear component parameter with less dependency on a priori knowledge of the accuracy of the associated linear system. An iterative optimization process is developed for solving the calibration problem so that the model parameters can be calibrated with less computational cost and more accurate results compared to a discretized approach.

Work has also been conducted to quantify the influence of measurement noise, a reduced set of measurements, and model error location on the proposed method. These studies show that the method is quite robust against introduced measurement noise, especially in the calibration of the linear component parameter to the true value. In addition, as long as the structural response is measured close to the location of the nonlinearity, the method has shown calibration capability with a relatively scarce set of measured data points. The proposed method has been evaluated for a case that entails a spatially localized nonlinearity, there is room for further work in testing the approach in calibrating other types of nonlinearity, such as nonlinear material properties. One area for further work includes the natural extension of this approach in increasing the applied excitation in a gradual manner and assessing the residual energy between model predictions and the experimental measurements. This extension would expand the proposed approach from a "two-step" method to an iterative, multi-step approach. The authors believe that complicated systems could benefit from this iterative series of increasing excitations to gradually improve the predominately linear and then nonlinear model accuracy if the two responses cannot be clearly distinguished from one another with a single excitation step. This is certainly an area of further research in the development of a more universally applicable framework for nonlinear system identification and calibration.

References

Atamturktur, S., Gilligan, C. and Salyards, K. (2013), "Detection of internal defects in concrete members using global vibration characteristics", *Materials Journal (ACI)*, Vol. 110 No. 5, pp. 529-538.

Atamturktur, S., Hemez, F. and Laman, J. (2012), "Uncertainty quantification in model verification and validation as applied to large scale historic masonry monuments", *Engineering Structures*, Elsevier, Vol. 43, pp. 221-234.

Atamturktur, S. and Laman, J. (2012), "Finite element model correlation and calibration of historic monuments: Review", *The Structural Design of Tall and Special Buildings* , Wiley, Vol. 21 No. 2, pp. 96-113.

Bellizzi, S. and Defilippi, M. (2003), "Non-linear mechanical systems identification using linear systems with random parameters", *Mechanical Systems and Signal Processing*, Vol. 17 No. 1, pp. 203-210.

Böswald, M. and Link, M. (2004), "Identification of non-linear joint parameters by using frequency response residuals", in *Proceedings of the 2004 International Conference on Noise and Vibration Engineering (ISMA2004), Leuven*, *Belgium*, September, pp. 20-22.

Cardona, A., Coune, T., Lerusse, A. and Geradin, M. (1994), "A multiharmonic method for non-linear vibration analysis", *International Journal for Numerical Methods in Engineering*, Vol. 37 No. 9, pp. 1593-1608.

Charbonnel, P.E., Ladevèze, P., Louf, F. and Le Noac'h, C. (2013), "A robust CRE-based approach for model updating using in situ measurements", *Computers and Structures*, Vol. 129, pp. 63-73.

Clough, R.W. and Wilson, E.L. (1979), "Dynamic analysis of large structural systems with local nonlinearities", *Computer Methods in Applied Mechanics and Engineering*, Vol. 17, pp. 107-129.

Deraemaeker, A., Ladevèze, P. and Leconte, P. (2002), "Reduced bases for model updating in structural dynamics based on constitutive relation error", *Computer Methods in Applied Mechanics and Engineering*, Vol. 191 Nos 21/22, pp. 2427-2444.

Ewins, D.J., Weekes, B. and Delli Carri, A. (2015), "Modal testing for model validation of structures with discrete nonlinearities", *Philosophical Transactions of the Royal Society A: Mathematical, Physical and Engineering Sciences*, Vol. 373 No. 2051, pp. 20140410.

Ferreira, J.V. and Serpa, A.L. (2005), "Application of the arc-length method in nonlinear frequency response", *Journal of Sound and Vibration*, Vol. 284 Nos 1/2, pp. 133-149.

Ferri, A.A. (1986), "On the equivalence of the incremental harmonic balance method and the harmonic balance-Newton raphson method", *Journal of Applied Mechanics*, Vol. 53 No. 2, pp. 455-457.

Ferri, A.A. and Dowell, E.H. (1988), "Frequency domain solutions to multi-degree-of-freedom, dry friction damped systems", *Journal of Sound and Vibration*, Vol. 124 No. 2, pp. 207-224.

Fey, R.H.B. (1992), *Steady-state Behaviour of Reduced Dynamic Systems with Local Nonlinearities*, Technische Universiteit, Eindhoven.

Fey, R.H.B., Van Campen, D.H. and De Kraker, A. (1996), "Long term structural dynamics of mechanical systems with local nonlinearities", *Journal of Vibration and Acoustics*, Vol. 118 No. 2, pp. 147-153.

Gondhalekar, A.C., Petrov, E.P. and Imregun, M. (2009), "Parameters identification for nonlinear dynamic systems via genetic algorithm optimization", *Journal of Computational and Nonlinear Dynamics*, Vol. 4 No. 4, p. 041002.

Guyan, R.J. (1965), "Reduction of stiffness and mass matrices", *AIAA Journal*, Vol. 3 No. 2, p. 380.

Hot, A. (2012), Validation expérimentale de structures localement non-linéaires dans un contexte spatial, Doctoral dissertation, Besançon.

Hu, X., Prabhu, S., Atamturktur, S. and Cogan, S. (2017), "Mechanistically-informed damage detection using dynamic measurements: Extended constitutive relation error", *Mechanical Systems and Signal Processing*, Vol. 85, pp. 312-328.

Huang, S., Petrov, E.P. and Ewins, D.J. (2006), "Comprehensive analysis of periodic regimes of forced vibration for structures with nonlinear snap-through springs", *Applied Mechanics and Materials*, Vol. 5 No. 6, pp. 3-13.

Isasa, I., Hot, A., Cogan, S. and Sadoulet-Reboul, E. (2011), "Model updating of locally non-linear systems based on multi-harmonic extended constitutive relation error", *Mechanical Systems and Signal Processing*, Vol. 25 No. 7, pp. 2413-2425.

Jaishi, B. and Ren, W.X. (2007), "Finite element model updating based on eigenvalue and strain energy residuals using multiobjective optimisation technique", *Mechanical Systems and Signal Processing*, Vol. 21 No. 5, pp. 2295-2317.

Kerschen, G., Golinval, J.C., Vakakis, A.F. and Bergman, L.A. (2005), "The method of proper orthogonal decomposition for dynamical characterization and order reduction of mechanical systems: an overview", *Nonlinear Dynamics*, Vol. 41 Nos 1/3, pp. 147-169.

Kerschen, G., Lenaerts, V. and Golinval, J.C. (2003), "Identification of a continuous structure with a geometrical non-linearity. Part I: Conditioned reverse path method", *Journal of Sound and Vibration*, Vol. 262 No. 4, pp. 889-906.

Kerschen, G., Peeters, M., Golinval, J.C. and Vakakis, A.F. (2009), "Nonlinear normal modes, Part I: A useful framework for the structural dynamicist", *Mechanical Systems and Signal Processing*, Vol. 23 No. 1, pp. 170-194.

Kerschen, G., Worden, K., Vakakis, A.F. and Golinval, J.C. (2006), "Past, present and future of nonlinear system identification in structural dynamics", *Mechanical Systems and Signal Processing*, Vol. 20 No. 3, pp. 505-592.

Kim, G.H. and Park, Y.S. (2004), "An improved updating parameter selection method and finite element model update using multiobjective optimisation technique", *Mechanical Systems and Signal Processing*, Vol. 18 No. 1, pp. 59-78.

Ladevèze, P. and Leguillon, D. (1983), "Error estimate procedure in the finite element method and applications", *SIAM Journal on Numerical Analysis*, Vol. 20 No. 3, pp. 485-509.

Larsson, A. and Abrahamsson, T. (1999), "A comparison of finite element model error localization methods", In *IMAC XVII-17th International Modal Analysis Conference-Modal Analysis: Reducing the Time to Market*, pp. 929-935.

Lenaerts, V., Kerschen, G. and Golinval, J.C. (2001), "Proper orthogonal decomposition for model updating of non-linear mechanical systems", *Mechanical Systems and Signal Processing*, Vol. 15 No. 1, pp. 31-43.

Leung, A.Y.T. and Fung, T.C. (1989), "Phase increment analysis of damped duffing oscillators", *International Journal for Numerical Methods in Engineering*, Vol. 28 No. 1, pp. 193-209.

Llau, A., Jason, L., Dufour, F. and Baroth, J. (2015), "Adaptive zooming method for the analysis of large structures with localized nonlinearities", *Finite Elements in Analysis and Design*, Vol. 106, pp. 73-84.

Majumder, L. and Manohar, C.S. (2003), "A time-domain approach for damage detection in beam structures using vibration data with a moving oscillator as an excitation source", *Journal of Sound and Vibration*, Vol. 268 No. 6, pp. 699-716.

Masri, S.F. and Caughey, T. (1979), "A nonparametric identification technique for nonlinear dynamic problems", *Journal of Applied Mechanics*, Vol. 46 No. 2, pp. 433-447.

Meyer, S. and Link, M. (2003), "Modelling and updating of local non-linearities using frequency response residuals", *Mechanical Systems and Signal Processing*, Vol. 17 No. 1, pp. 219-226.

Moaveni, B. and Asgarieh, E. (2012), "Deterministic-stochastic subspace identification method for identification of nonlinear structures as time-varying linear systems", *Mechanical Systems and Signal Processing*, Vol. 31, pp. 40-55.

Nelson, H.D. and Nataraj, C. (1989), "Periodic solutions in rotor dynamic systems with nonlinear supports: a general approach", *Journal of Vibration Acoustics Stress and Reliability in Design*, Vol. 111, pp. 187-193.

Niwa, A. and Clough, R.W. (1982), "Non-linear seismic response of arch dams", *Earthquake Engineering and Structural Dynamics*, Vol. 10 No. 2, pp. 267-281.

Nocedal, J. and Wright, S. (2006), *Numerical Optimization*, Springer Science and Business Media.

Qu, Z.Q. (2002), "Model reduction for dynamical systems with local nonlinearities", *AIAA Journal*, Vol. 40 No. 2, pp. 327-333.

Ren, Y., Lim, T.M. and Lim, M.K. (1998), "Identification of properties of nonlinear joints using dynamic test data. Transactions-ASME", *Journal of Vibration and Acoustics*, Vol. 120 No. 2, pp. 324-330.

Shi, G. and Atluri, S.N. (1992), "Nonlinear dynamic response of frame-type structures with hysteretic damping at the joints", *AIAA Journal*, Vol. 30 No. 1, pp. 234-240.

Stoker, J.J. (1950), *Nonlinear Vibrations in Mechanical and Electrical Systems*, Interscience Publishers, New York, NY.

Stricklin, J.A. and Haisler, W.E. (1977), "Formulations and solution procedures for nonlinear structural analysis", *Computers and Structures*, Vol. 7, pp. 125-136.

Tamura, H., Tsuda, Y. and Sueoka, A. (1981), "Higher approximation of steady oscillations in nonlinear systems with single degree of freedom: Suggested multi-harmonic balance method", *Bulletin of JSME*, Vol. 24 No. 195, pp. 1616-1625.

Thouverez, F. (2003), "Presentation of the ECL benchmark", *Mechanical Systems and Signal Processing*, Vol. 17 No. 1, pp. 195-202.

Tondl, A. (1974), "Notes on the solution of forced oscillations of a third-order non-linear system", *Journal of Sound and Vibration*, Vol. 37 No. 2, pp. 273-279.

Vakakis, A.F. (1997), "Non-linear normal modes (NNMs) and their applications in vibration theory: an overview", *Mechanical Systems and Signal Processing*, Vol. 11 No. 1, pp. 3-22.

Van Buren, K. and Atamturktur, S. (2012), "A comparative study: Predictive modeling of wind turbine blades. Journal of ", *Wind Engineering*, Vol. 36 No. 3, pp. 235-250.

Wilson, E.L., Farhoomand, I. and Bathe, K.J. (1972), "Nonlinear dynamic analysis of complex structures", *Earthquake Engineering and Structural Dynamics*, Vol. 1 No. 3, pp. 241-252.

Wojtkiewicz, S.F. and Johnson, E.A. (2011), "Efficient uncertainty quantification of dynamical systems with local nonlinearities and uncertainties", *Probabilistic Engineering Mechanics*, Vol. 26 No. 4, pp. 561-569.

Worden, K. (2003), "Cost action F3 on structural dynamics: benchmarks for working group 2 – structural health monitoring", *Mechanical Systems and Signal Processing*, Vol. 17 No. 1, pp. 73-75.

Worden, K. and Tomlinson, G.R. (2000), *Nonlinearity in Structural Dynamics: detection, identification and Modelling*, CRC Press.

Yu, E., Taciroglu, E. and Wallace, J.W. (2007), "Parameter identification of framed structures using an improved finite element model-updating method – Part I: formulation and verification", *Earthquake Engineering and Structural Dynamics*, Vol. 36 No. 5, pp. 619-639.

Zimmerman, D.C. and Kaouk, M. (1994), "Structural damage detection using minimum rank update theory", *Journal of Vibration and Acoustics*, Vol. 116 No. 2, pp. 222-231.

Further reading

Kurt, M., Eriten, M., McFarland, D.M., Bergman, L.A. and Vakakis, A.F. (2015), "Methodology for model updating of mechanical components with local nonlinearities", *Journal of Sound and Vibration*, Vol. 357, pp. 331-348.

Schultze, J.F., Hemez, F.M., Doebling, S.W. and Sohn, H. (2001), "Application of non-linear system model updating using feature extraction and parameter effects analysis", *Shock and Vibration*, Vol. 8 No. 6, pp. 325-337.

Stevens, G., Atamturktur, S., Lebensohn, R. and Kaschner, G. (2016), "Experiment-based validation and uncertainty quantification of coupled multi-scale plasticity models", *Multidiscipline Modeling in Materials and Structures*, Vol. 12 No. 1, pp. 151-176.

Corresponding author
Sez Atamturktur can be contacted at: sez@psu.edu